Vibrational Predissociation Spectroscopic and Ab Initio Theoretical Studies on Protonated Ethylenediamine−$(Water)_3$ Complex

Kwang-Yon Kim,[†] Huan-Cheng Chang,[‡] Yuan T. Lee,[‡] Ung-In Cho,[†] and Doo Wan Boo*[,†]

Department of Chemistry, Yonsei University, Seoul 120-749, Korea, and Institute of Atomic and Molecular Sciences, Academia Sinica, P.O. Box 23-166, Taipei, Taiwan, R.O.C.

Received: January 6, 2003; In Final Form: March 28, 2003

Structures, interactions, and vibrations of an intramolecular hydrogen bond (IHB)-containing protonated ion−$(water)_3$ complex, *g*-$enH^+(H_2O)_3$ (*g*-enH^+ = *gauche*-protonated ethylenediamine) and *t*-$enH^+(H_2O)_3$ (*t*-enH^+ = *trans*-protonated ethylenediamine) with no IHB were investigated by combined vibrational predissociation spectroscopy and ab initio calculations. The observed vibrational feature at 3552 cm^{-1} (signature of cyclic ion−$(water)_3$ structure), consistent with ab initio results on the stabilities of structural isomers, suggested the IHB-assisted bicyclic structure for *g*-$enH^+(H_2O)_3$. Ab initio many-body analyses further indicated that the greater stability of bicyclic isomer versus monocyclic and bicyclic tripod isomers originates from the destabilization of the latter by the large relaxation energies and repulsive nonadditive interactions. The close correlation between the observed and calculated vibrational spectra for *g*-$enH^+(H_2O)_3$ revealed the coexistence of bicyclic isomers and monocyclic open isomers in our beam, consistent with the trend of the calculated Gibbs free energies at 150 K.

I. Introduction

The intramolecular hydrogen bonding (IHB) in ionic chromophores and the intermolecular hydrogen bonding with surrounding water molecules, particularly in the first few solvation shells, are of biological significance in protonated peptides and ionic intermediates in enzyme processes.[1] In recent decades, ab initio theoretical,[2,3] gas-phase mass spectrometric,[3,4] and spectroscopic[5] studies on size-selected, protonated ion−water complexes have provided a detailed understanding of ion−water and water−water interactions, and of the structural evolution with increasing number of water molecules. The structural trends of protonated ion−$(water)_n$ complexes are markedly different from those of neutral water clusters[6] and anionic core−$(water)_n$ complexes[7] that preferentially form cyclic structures for the most sizes of complexes. For $R-NH_3^+(H_2O)_n$ (R = H, CH_3; n = 1, 2, 3...), for instance, the charge−dipole interactions between the protons of the $-NH_3^+$ group and the H_2O molecules are dominant for the first solvation shell (referred to as $1°H_2O$) forming a noncyclic "tripod" structure for n = 3.[2,8] Cyclic hydrated structures formed by hydrogen bonding between $1°H_2O$ and $2°H_2O$ molecules have been observed exclusively when the number of H_2O molecules in the complexes are greater than the number of protons in the ion core.[8,9]

This structural trend may change in the hydration of a protonated ion with IHBs due to strong IHB−$1°H_2O$ interactions as suggested by the studies on neutral IHB-containing chromophore−$(water)_n$ clusters.[10] With the use of vibrational predissociation (VP) spectroscopy and ab initio quantum calculations, we attempted in this work to elucidate the structures and stabilities, and intracluster interactions of IHB-containing *gauche*-protonated ethylenediamine−$(water)_3$ complexes, *g*-$enH^+(H_2O)_3$ (*g*-enH^+= *gauche*-$NH_2CH_2CH_2NH_3^+$) and the corresponding trans-form with no IHB, *t*-$enH^+(H_2O)_3$ (*t*-enH^+ = *trans*-$NH_2CH_2CH_2NH_3^+$).

For free protonated ethylenediamine in the gas phase, the gauche-form is known to be more stable than the trans-form by ∼10 kcal/mol.[11,12] Preliminary ab initio calculations on *g*-, *t*-$enH^+(H_2O)_3$ also predicted that the gauche-form is lower in energy than the trans-form by 6∼7 kcal/mol.[12] This suggested an exclusive population of *g*-$enH^+(H_2O)_3$ over *t*-$enH^+(H_2O)_3$ when the complexes are synthesized in a cold supersonic jet. In this paper, we report our vibrational predissociation spectroscopic and ab initio results on protonated ethylenediamine−$(water)_3$ complexes in an effort to understand the hydration behavior of an IHB-containing protonated ion core.

II. Methods

A. Vibrational Predissociation Spectroscopy. The experiment was conducted using a vibrational predissociation ion trap (VPIT) spectrometer. Details of the apparatus have been previously described.[13] Briefly, we synthesized protonated ethylenediamine−$(water)_n$ complexes by a low current, low-temperature corona discharge of ethylenediamine/H_2O gas mixture seeded in pure H_2 at the pressure of ∼150 Torr, and subsequent supersonic expansion. The discharge currents used were ≤10 μA, and the temperature of source body in contact with a liquid nitrogen trap was maintained at ∼150 K. The rotational and vibrational temperatures under these conditions were expected to be ∼50 and ∼150 K, respectively.[8,14] The $enH^+(H_2O)_3$ ions were mass-selected by a sector magnet and then stored in an octapole ion trap for 1∼2 ms for ion accumulation and cooling of internally hot ions before infrared irradiation. A quadrupole mass spectrometer equipped with a Daly detector operated in ion counting modes, selectively detected the fragment ions, $enH^+(H_2O)_2$ upon infrared irradiation to obtain virtually background-free spectra. The excitation was made by a pulsed infrared laser, generated by difference

* To whom correspondence should be addressed; Tel: +82-2-2123-2632. Fax: +82-2-364-7050. E-mail: dwboo@alchemy.yonsei.ac.kr.
[†] Yonsei University.
[‡] Academia Sinica.

10.1021/jp034024e CCC: $25.00
Published on Web 06/03/2003

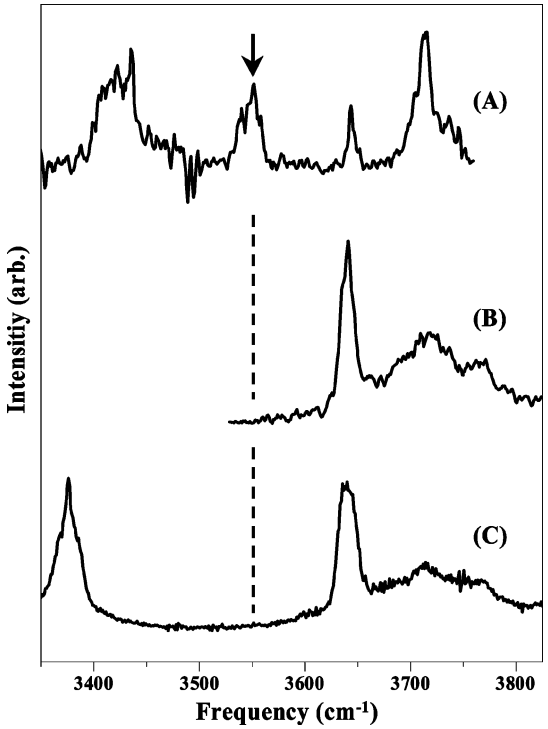

Figure 1. Vibrational predissociation spectra of (A) *g*-enH$^+$(H$_2$O)$_3$; (B) CH$_3$NH$_3^+$(H$_2$O)$_3$; and (C) NH$_4^+$(H$_2$O)$_3$. *g*-enH$^+$ = *gauche*-protonated ethylenediamine or *gauche*-NH$_2$CH$_2$CH$_2$NH$_3^+$. Note that the characteristic band and frequency region for the cyclic ion−(water)$_3$ structure are denoted by an arrow and dashed lines.

frequency mixing of Nd:YAG laser and dye laser photons. Since the hydration energy by third H$_2$O molecule in enH$^+$(H$_2$O)$_3$ is ∼11 kcal/mol,[12,15] one or two infrared photons in the range of 3000∼3800 cm^{-1} used in this work are sufficient to dissociate enH$^+$(H$_2$O)$_3$ into enH$^+$(H$_2$O)$_2$ and one H$_2$O molecule.

B. Ab Initio Quantum Calculations. Ab initio quantum computations on *g*-, *t*-enH$^+$(H$_2$O)$_3$ at MP2(full)/6-31+G(d), MP2(full)/6-311++G(d,p), MP4(SDTQ)/6-311++G(d,p), and B3LYP/6-31+G(d) levels were performed using the Gaussian-98 program.[16] The geometries were optimized using analytical gradients at MP2(full)/6-31+G(d) and B3LYP/6-31+G(d) and the vibrational frequencies were obtained using analytical second derivatives at MP2(full)/6-311++G(d,p) and B3LYP/6-31+G(d) levels. The scaling factors for the calculated frequencies at MP2(full)/6-311++G(d,p) and B3LYP/6-31+G(d) were 0.981 and 0.973 determined by referring to the experimentally observed antisymmetric free O−H stretching frequency.[8] The calculated total hydration energies, enthalpies, and Gibbs free energies were corrected by zero-point vibrational energy (ZPVE) and basis set superposition errors (BSSE) following the procedures of Boys−Bernardi.[17] Finally, many-body (MB) analyses of hydration interactions were also carried out following the works of Stillinger, Kim, and Xantheas.[12,18]

III. Results and Discussion

A. Vibration Predissociation Spectra. Figure 1 shows the observed VP spectrum for the protonated ethylenediamine−(water)$_3$ complex in the frequency region of 3350∼3820 cm^{-1} along with the spectra for CH$_3$NH$_3^+$(H$_2$O)$_3$ and NH$_4^+$(H$_2$O)$_3$. Four vibrational features centered at 3714, 3642, 3552, 3435 cm^{-1} were found. Of considerable interest was the intense doublet feature at 3552 cm^{-1} in the spectrum that has no counterparts for CH$_3$NH$_3^+$(H$_2$O)$_3$ and NH$_4^+$(H$_2$O)$_3$ (marked by arrow and dashed lines). The similar vibrational features at

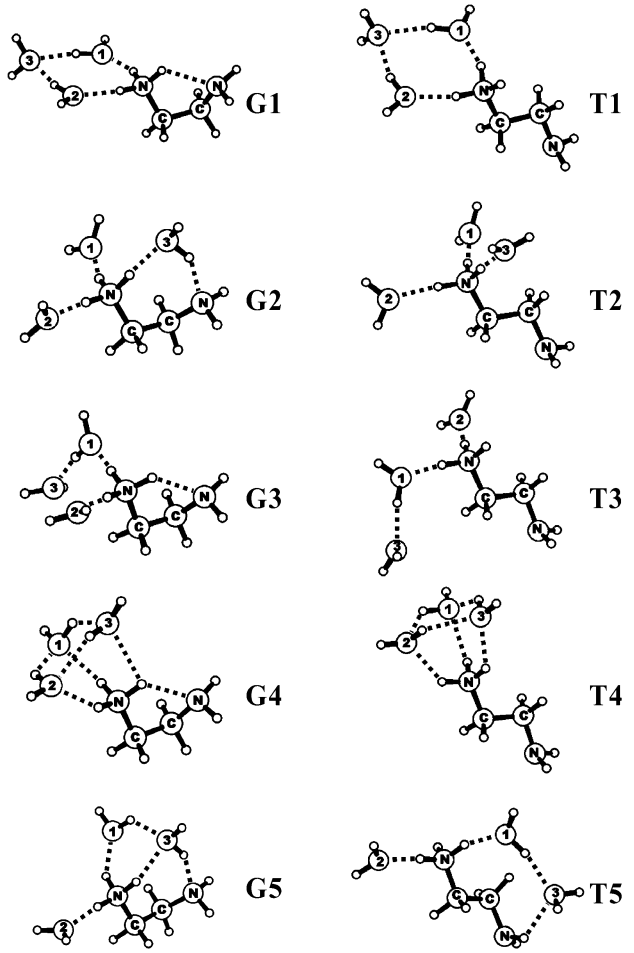

Figure 2. Ab initio optimized structural isomers for *g*-enH$^+$(H$_2$O)$_3$ (**G1**−**G5**) and *t*-enH$^+$(H$_2$O)$_3$ (**T1**−**T5**) at MP2(full)/6-31+G(d).

∼3550 cm^{-1} have been previously reported mainly for large protonated ion−water complexes such as NH$_4^+$(H$_2$O)$_n$ ($n \geq 5$) and CH$_3$NH$_3^+$(H$_2$O)$_n$ ($n \geq 4$) after the first solvation shells were completed. They were attributed to the symmetric and antisymmetric bonded O−H stretches of two 1°H$_2$O molecules bonded by one 2°H$_2$O molecule in a cyclic form of core ion−(H$_2$O)$_3$ moiety.[8,9] This suggested a cyclic hydrated structure for the protonated ethylenediamine−(water)$_3$ complex, particularly *g*-enH$^+$(H$_2$O)$_3$. This result was further supported by the intensity pattern for 3642, 3714 cm^{-1} bands for *g*-enH$^+$(H$_2$O)$_3$ that are different from those of NH$_4^+$(H$_2$O)$_3$ and CH$_3$NH$_3^+$(H$_2$O)$_3$, but similar to those of NH$_4^+$(H$_2$O)$_n$ ($n \geq 5$) and CH$_3$NH$_3^+$(H$_2$O)$_n$ ($n \geq 4$).[8,9] The different hydration behavior between *g*-enH$^+$ core and protonated ion cores with no IHB suggests an important role of the IHB−1°H$_2$O interactions in determining the structures and stabilities of protonated ion−water complexes.

B. Ab Initio Geometries, Energetics, and Thermodynamics. A number of local minimum energy structures exist in the multidimensional potential energy surfaces of *g*-, *t*-enH$_3^+$(H$_2$O)$_3$. Figure 2 depicts 10 representative isomeric structures optimized at MP2(full)/6-31+G(d), **G1**−**G5** for *g*-enH$^+$(H$_2$O)$_3$ and **T1**−**T5** for *t*-enH$^+$(H$_2$O)$_3$.[19] Six isomers (**G1**−**G3**, **T1**−**T3**) among these isomers have been previously studied at the B3LYP/6-31+G(d) level.[12] The calculated electronic energies and total hydration energies for 10 isomers at various levels with and without ZPVE- and BSSE-corrected are listed in Table 1. The ZPVE- and BSSE-corrected energies at MP2(full)/6-311++G(d,p) are mainly discussed in this work. The thermodynamic functions such as total hydration enthalpies and total hydration

TABLE 1: Electronic Energies (E_{el}) and Total Hydration Energies (ΔE_{hyd}) for Structrural Isomers of *g*-, *t*-enH$^+$(H$_2$O)$_3$ at MP2(full)/6-31+G(*d*), MP2(full)/6-311++G(*d,p*), and MP4(SDTQ)/6-311++G(*d,p*)[a]

	MP2(full)/6-31+G(*d*)			MP2(full)/6-311++G(*d,p*)			MP4(SDTQ)/6-311++G(*d,p*)
	E_{el}	$E_{el,ZPVE,BSSE}$	ΔE_{hyd}	E_{el}	$E_{el,ZPVE,BSSE}$	ΔE_{hyd}	E_{el}
G1	−418.985442	−418.773558	−39.34	−419.423565	−419.211327	−34.26	−419.533170
	(0.00)	(0.00)	(4.25)	(0.00)	(0.00)	(4.11)	(0.00)
G2	−418.982058	−418.770545	−37.45	−419.421354	−419.208517	−32.50	−419.531136
	(2.12)	(1.89)	(6.14)	(1.39)	(1.76)	(5.88)	(1.14)
G3	−418.981412	418.772717	−38.81	−419.420941	−419.210170	−33.54	−419.530434
	(2.53)	(0.53)	(4.78)	(1.65)	(0.73)	(4.84)	(1.72)
G4	−418.981789	−418.769618	−36.87	−419.419027	−419.205376	−30.53	
	(2.29)	(2.47)	(6.72)	(2.85)	(3.73)	(7.85)	
G5	−418.984385	−418.770816	−37.62	−419.422351	−419.208221	−32.31	
	(0.66)	(1.72)	(5.97)	(0.76)	(1.95)	(6.06)	
T1	−418.972834	−418.761389	−42.25	−419.411835	−419.199918	−37.36	
	(7.91)	(7.64)	(1.35)	(7.36)	(7.16)	(1.02)	
T2	−418.970519	−418.763533	−43.59	−419.410966	−419.201544	−38.38	
	(9.36)	(6.29)	(0.00)	(7.91)	(6.14)	(0.00)	
T3	−418.968552	−418.760540	−41.71	−419.408961	−419.198732	−36.61	
	(10.60)	(8.17)	(1.88)	(9.16)	(7.90)	(1.76)	
T4	−418.969694	−418.758339	−40.33	−419.407657	−419.194635	−34.04	
	(9.88)	(9.55)	(3.26)	(9.98)	(10.47)	(4.34)	
T5	−418.968915	−418.759573	−41.11	−419.409021	−419.197896	−36.09	
	(10.37)	(8.78)	(2.49)	(9.13)	(8.43)	(2.29)	

[a] All the absolute energies are in hartree, and the relative energies and total hydration energies are in kcal/mol.

TABLE 2: Total Hydration Enthalpies (ΔH_{hyd}) and Gibbs Free Energies (ΔG_{hyd}) for Structural Isomers of *g*-, *t*-enH$^+$(H$_2$O)$_3$ for the Clustering Reaction *g*-, *t*-enH$^+$ + 3H$_2$O → *g*-, *t*-enH$^+$(H$_2$O)$_3$ at 298 and 150 K[a]

	MP2(full)/6-31+G(*d*)				MP2(full)/6-311++G(*d,p*)			
	$\Delta H_{hyd,298K}$	$\Delta H_{hyd,150K}$	$\Delta G_{hyd,298K}$	$\Delta G_{hyd,150K}$	$\Delta H_{hyd,298K}$	$\Delta H_{hyd,150K}$	$\Delta G_{hyd,298K}$	$\Delta G_{hyd,150K}$
G1	−40.69	−41.06	−14.89	−27.86	−36.56	−36.35	−8.28	−22.32
	(0.00)	(0.00)	(2.45)	(0.68)	(0.00)	(0.00)	(0.26)	(0.00)
G2	−38.26	−38.87	−14.50	−26.53	−34.69	−34.56	−6.73	−20.64
	(2.43)	(2.19)	(2.84)	(2.02)	(1.86)	(1.79)	(1.82)	(1.68)
G3	−39.41	−40.08	−17.34	−28.54	−35.58	−35.49	−8.54	−22.00
	(1.28)	(0.98)	(0.00)	(0.00)	(0.98)	(0.86)	(0.00)	(0.32)
G4	−38.64	−38.82	−11.52	−25.10	−33.02	−32.70	−4.09	−18.42
	(2.05)	(2.24)	(5.81)	(3.44)	(3.54)	(3.65)	(4.45)	(3.90)
G5	−39.06	−39.37	−13.02	−26.10	−34.78	−34.50	−5.86	−20.20
	(1.63)	(1.69)	(4.31)	(2.44)	(1.77)	(1.85)	(2.68)	(2.12)
T1	−43.83	−44.07	−17.61	−30.75	−39.80	−39.50	−11.29	−25.42
	(0.08)	(0.68)	(4.05)	(2.25)	(0.54)	(0.82)	(2.08)	(1.40)
T2	−43.90	−44.75	−21.66	−33.00	−40.34	−40.33	−13.37	−26.82
	(0.00)	(0.00)	(0.00)	(0.00)	(0.00)	(0.00)	(0.00)	(0.00)
T3	−42.54	−43.10	−19.68	−31.25	−38.79	−38.63	−11.48	−25.06
	(1.36)	(1.64)	(1.98)	(1.75)	(1.55)	(1.70)	(1.88)	(1.76)
T4	−42.33	−42.38	−14.80	−28.55	−36.67	−36.26	−7.61	−21.98
	(1.57)	(2.36)	(6.86)	(4.45)	(3.67)	(4.07)	(5.75)	(4.84)
T5	−42.15	−42.63	−17.80	−30.09	−38.36	−38.16	−10.35	−24.26
	(1.75)	(2.11)	(3.86)	(2.91)	(1.98)	(2.16)	(3.02)	(2.56)

[a] All values are in kcal/mol.

Gibbs free energies at 298 and 150 K were also calculated (Table 2). The relative Gibbs free energies were used to predict the relative populations of various isomers at 298 and 150 K.[19]

B.1. Geometries. As shown in Figure 2, the isomers **G1** and **T1** represent the cyclic hydrated isomers in which the third H_2O molecule (denoted as $H_2O(3)$) plays a role of proton double acceptor (AA), forming overall "bicyclic" and "monocyclic" structures, respectively. The five-membered IHB ring in **G1** is slightly modified from that of free *g*-enH$^+$ core evidenced by the dihedral angles ($\angle N^+CCN = 51.1°$ vs 43.8°). The hydrogen bond distances and angles for the core-1°H_2O moiety of **G1** increased from those of **T1**, whereas those for 1°H_2O−2°H_2O moieties are almost identical.[19] This suggests that the conformational difference (gauche, trans) in the ion core have influence on the first hydration shell but little on the second shell.

G2 and **T2** represent the "tripod" ion−$(H_2O)_3$ structures in which three H_2O molecules are bonded one-to-one to three protons of ion core, forming overall "monocyclic tripod" and "noncyclic tripod" structures, respectively. Of interest is that the $H_2O(3)$ in **G2** bonded to the IHB proton breaks into the five-membered IHB ring resulting in a H_2O-mediated seven-membered IHB ring. Many attempts to locate the $H_2O(3)$ exterior to the IHB ring converged to the same structure. The highly distorted seven-membered IHB ring of **G2** with a much increased dihedral angle ($\angle N^+CCN = 71.4°$) from that of free *g*-enH$^+$ core suggests strong interference between IHB and hydration interactions. Furthermore, the hydrogen bond distance for the core−$H_2O(3)$ moiety in **G2** is somewhat shortened from those for the core−$H_2O(1,2)$ moiety suggesting stronger core−ligand interactions for 1°$H_2O(3)$ directly bonded to the IHB proton than 1°$H_2O(1, 2)$ molecules.[19]

G3 and **T3** are open structural isomers formed by breaking the hydrogen bond between 1°$H_2O(2)$ and 2°$H_2O(3)$ from the corresponding cyclic isomers (**G1**, **T1**), and named as "mono-

cyclic open" and "noncyclic open" structures, respectively. The hydrogen bond distances for core−1°H_2O(1) and 1°H_2O(1)−2°H_2O(3) in **G3**, **T3** were somewhat shortened from those of **G1**, **T1** due to the enhanced hydrogen bond cooperativity, while the hydrogen bond distances for core−1°H_2O(2) were lengthened.[19] They are expected to be favorable at high temperatures due to the large entropy effects by their open structures.

G4 and **T4** represent the "caged" ion−$(H_2O)_3$ structures where the $-NH_3^+$ moieties are bound by cyclic water trimer, forming overall "monocyclic caged" and "noncyclic caged" structures, respectively. It was noticeable that the orientations of H_2O molecules and the ring size of cyclic water trimer moiety changed substantially from those of free cyclic water trimer.[6] As shown in Figure 2, the free O−H bonds of the -$(H_2O)_3$ moiety are directed away from the ion core for facile interactions between the protons of ion core and the lone electron pairs of H_2O molecules, resulting in a somewhat distorted hydrogen bond network.

G5 is a modified tripod structure from **G2** where the 1°H_2O-(3) of the seven-membered IHB ring forms additional hydrogen bond with adjacent 1°H_2O(1) by acting as proton double acceptor and single donor (AAD), and named as a "bicyclic tripod" structure. Such structure with a hydrogen bond between two 1°H_2O molecules could be induced by strong interactions between the IHB and 1°H_2O molecules. **T5** has an extended hydrogen bond structure that two H_2O(1,3) molecules bridge the remote $-NH_3^+$ and $-NH_2$ moieties in the *t*-enH$^+$ core by hydrogen bonding, and named as "water-bridged cyclic" structure.

B.2. Energetics. Table 1 lists the absolute electronic energies for 10 isomers, and their total hydration energies for the clustering reaction, *g*-, *t*-enH$^+$ + $3H_2O$ → *g*-, *t*-enH$^+(H_2O)_3$. Note that the numbers in parentheses are the relative energies with respect to isomer **G1** for absolute electronic energies and isomer **T2** for total hydration energies. As shown in Table 1, the gauche-isomers were predicted to be 6−10 kcal/mol lower in energy than trans-isomers due to the IHB-stabilization consistent with the previous work.[12]

The bicyclic isomer **G1** was lowest in energy among 10 isomers calculated in this work. The greater stability of the cyclic form (**G1**) vs the tripod form (**G2**) for *g*-enH$^+(H_2O)_3$ is different from the cases of non-IHB core−$(H_2O)_3$ complexes such as *t*-enH$^+(H_2O)_3$, $NH_4^+(H_2O)_3$, $CH_3NH_3^+(H_2O)_3$ in which the tripod isomers with greater charge−dipole interactions tend to be lowest in energy.[20,21] The open monocyclic isomer **G3** is ∼1 kcal/mol lower in energy than **G2**, but slightly higher in energy without ZPVE and BSSE corrections (Table 1). The monocyclic caged isomer **G4** and the bicyclic tripod isomer **G5** are 3.7 and 1.95 kcal/mol higher in energy than **G1**, respectively, due to the geometric constraints. Overall, the stability order for gauche-isomers was predicted to be **G1** > **G3** > **G2** ≈ **G5** > **G4**.

For trans-isomers, the noncyclic tripod isomer **T2** is the lowest energy isomer among five trans-isomers. It was predicted to be 1.0 and 1.8 kcal/mol lower in energy than the monocyclic isomer **T1** and the noncyclic open isomer **T3**, respectively. The noncyclic caged isomer **T4** and the water-bridged isomer **T5** are 4.3 and 2.3 kcal/mol higher in energy than **T2**. The overall stability orders for trans-isomers are **T2** > **T1** > **T3** > **T5** > **T4**.

The trends of the total hydration energies were different from those of the absolute electronic energies. The total hydration energies for gauche-isomers were 3−6 kcal/mol smaller than those of the corresponding trans-isomers due to strong interference between the IHB in *g*-enH$^+$ core and surrounding 1°H_2O molecules. The noncyclic tripod isomer **T2** with a maximum charge−dipole interaction has the largest hydration energy (−38.4 kcal/mol), while the monocyclic caged isomer **G4** with a cyclic water trimer unit has the smallest hydration energy (−30.5 kcal/mol). The extent of IHB-hydration interference for each type of structural isomer (cyclic, tripod, open, caged) can be determined by calculating the differences in the hydration energies between each gauche-isomers and corresponding trans-isomers. The calculated differential hydration energies (i.e., **G1**−**T1**, **G2**−**T2**, **G3**−**T3**, **G4**−**T4**) were 3.1, 5.9, 3.1, 3.5 kcal/mol, respectively, suggesting the strongest IHB-hydration interference for the monocyclic tripod isomer **G2**.

B.3. Thermodynamics. Table 2 illustrates the calculated total hydration enthalpies (ΔH_{hyd}) and total hydration Gibbs free energies (ΔG_{hyd}) at 298 and 150 K. The calculated total hydration enthalpy of the lowest energy isomer **G1** at MP2(full)/6-311++G(d,p) (−36.4 kcal/mol) is in close proximity to the experimental value (−37.7 kcal/mol) at 298 K.[15] It was found that the *g*-enH$^+(H_2O)_3$ isomers have smaller total hydration enthalpies and total Gibbs free energies by 3−6 kcal/mol than the corresponding *t*-enH$^+(H_2O)_3$ isomers, similar to the trends of total hydration energies.

The relative populations of various isomers can be determined by calculating their relative Gibbs free energies.[19] As shown in Table 2, the monocyclic open isomer **G3** with a flexible structure has lowest Gibbs free energy at 298 K due to the large entropy contribution, while at 150 K, the ground-state isomer **G1** has lowest Gibbs free energy. The other isomers were predicted to have higher Gibbs free energies than **G1**, **G3** at 298 and 150 K, suggesting that the isomers **G1** and **G3** would have larger populations at both temperatures, and contribute predominantly to the experimentally observed vibrational predissociation spectrum.

C. Vibration Spectral Analysis. Table 3 lists the calculated vibrational frequencies, intensities, and the vibrational assignments for isomers **G1**−**G5** at MP2(full)/6-311++G(d,p) in the 3000∼3800 cm^{-1} frequency range. The thermodynamically less stable trans-isomers were not likely to contribute to the observed spectrum, so they were ignored in this work. The calculated stick spectra for isomers **G1**−**G5** and the experimentally observed spectrum are compared in Figure 3. Six vibrational features centered at 3714, 3642, 3552, 3435, ∼3152, and ∼3100 cm^{-1} were found in the experimental spectrum. The first two bands were assigned to the typical antisymmetric and symmetric free O−H stretches of H_2O molecules in water-solvated ionic complexes.[5,8] The observed sharp feature for antisymmetric stretch correlates with the stick spectrum for the bicyclic isomer **G1**. As mentioned previously, the 3552 cm^{-1} doublet, signature of cyclic ion-(water)$_3$ complex, was assigned to the antisymmetric and symmetric bonded O−H stretches of two 1°H_2O molecules of **G1** (3526, 3507 cm^{-1}).

The 3435 cm^{-1} band that is not seen in spectrum of **G1** correlates well with the bonded O−H stretch of 1°H_2O of **G3** (3422 cm^{-1}), indicating significant population of the monocyclic open isomer **G3** besides the bicyclic isomer **G1** in our beam. This experimental finding is consistent with the similar Gibbs free energies predicted for **G1** and **G3** at 150 K (Table 2). Note that for $NH_4^+(H_2O)_3$ and $CH_3NH_3^+(H_2O)_3$, the noncyclic tripod isomer like **T2** was always the most predominant species at both 298 and 150 K.[20,21]

The vibrational features centered at ∼3152, ∼3100 cm^{-1} in the spectrum are located within the frequency range of the IHB

TABLE 3: Ab Initio Scaled Frequencies (cm^{-1}), IR Absorption Intensities (km/mol), and Assignments for C−H, N−H, and O−H Stretches of *g*-enH$^+$(H$_2$O)$_3$ at MP2(full)/6-311++G(*d,p*)

frequency	intensity	assignments[a]	frequency	intensity	assignments[a]
			G1 Isomer		
3716	54	symmetric free-OH(1,2)	3290	432	bonded-N$^+$H
3715	142	antisymmetric free-OH$_2$(3)	3199	466	antisymmetric bonded-N$^+$H$_2$(1,2)
3713	296	antisymmetric free-OH(1,2)	3170	577	symmetric bonded-N$^+$H$_3$
3609	10	symmetric free-OH$_2$(3)	3136	6	antisymmetric CH$_2$(N$^+$)
3530	25	antisymmetric free-NH$_2$	3085	14	antisymmetric CH$_2$(N)
3526	512	symmetric bonded-OH(1,2)	3066	5	symmetric CH$_2$(N$^+$)
3507	213	antisymmetric bonded-OH(1,2)	3025	16	symmetric CH$_2$(N)
3441	11	symmetric free-NH$_2$			
			G2 Isomer		
3738	141	antisymmetric free-OH(2)	3249	776	antisymmetric bonded-N$^+$H$_2$(1,2)
3733	126	antisymmetric free-OH(1)	3208	504	symmetric bonded-N$^+$H$_2$(1,2)
3709	154	free-OH(3)	3122	5	antisymmetric CH$_2$(N$^+$)
3626	41	symmetric free-OH(2)	3088	18	antisymmetric CH$_2$(N)
3620	42	symmetric free-OH(1)	3079	492	bonded-N$^+$H(3)
3496	20	antisymmetric free-NH$_2$	3057	75	symmetric CH$_2$(N$^+$)
3414	11	symmetric free-NH$_2$	3015	15	symmetric CH$_2$(N)
3370	509	bonded-OH(3)			
			G3 Isomer		
3745	128	antisymmetric free-OH(3)	3272	526	antisymmetric bonded-N$^+$H$_2$(N,2)
3740	132	antisymmetric free-OH(2)	3223	518	symmetric bonded-N$^+$H$_2$(N,2)
3707	139	free-OH(1)	3134	1	antisymmetric CH$_2$(N$^+$)
3630	29	symmetric free-OH(3)	3107	656	bonded-N$^+$H (1)
3627	41	symmetric free-OH(2)	3093	14	antisymmetric CH$_2$(N)
3531	24	antisymmetric free-N$^+$H$_2$	3064	31	symmetric CH$_2$(N$^+$)
3442	10	symmetric free-N$^+$H$_2$	3027	16	symmetric CH$_2$(N)
3422	571	bonded-OH(1)			
			G4 Isomer		
3714	153	free-OH(3)	3320	364	bonded-N$^+$H(2)
3705	156	free-OH(2)	3282	284	antisymmetric bonded-N$^+$H$_2$(1,3)
3699	191	free-OH(1)	3230	167	symmetric bonded-N$^+$H$_3$
3575	106	bonded-OH(3)	3135	4	antisymmetric CH$_2$(N$^+$)
3557	106	bonded-OH(2)	3084	12	antisymmetric CH$_2$(N)
3529	25	antisymmetric free-NH$_2$	3066	2	symmetric CH$_2$(N$^+$)
3497	158	bonded-OH(1)	3025	15	symmetric CH$_2$(N)
3441	12	symmetric free-NH$_2$			
			G5 Isomer		
3736	139	antisymmetric free-OH(2)	3241	626	bonded-OH(3) and antisymmetric bonded-N$^+$H$_3$
3715	163	free-OH(1)	3226	506	antisymmetric bonded-N$^+$H$_3$
3690	150	free-OH(3)	3179	241	symmetric bonded-N$^+$H$_3$
3625	44	symmetric free-OH(2)	3126	6	antisymmetric CH$_2$(N$^+$)
3541	159	bonded-OH(1)	3094	3	antisymmetric CH$_2$(N)
3489	20	antisymmetric free-NH$_2$	3061	8	symmetric CH$_2$(N$^+$)
3408	8	symmetric free-NH$_2$	3018	19	symmetric CH$_2$(N)
3292	650	bonded-OH(3) and antisymmetric bonded-N$^+$H$_3$			

[a] Numbers in parentheses denote numbers of H$_2$O molecules in the clusters according to Figure 1.

N−H stretch (3290 cm^{-1}) and 1°H$_2$O-bonded N−H stretches (3199, 3170 cm^{-1}) for **G1**, and the 1°H$_2$O-bonded N−H stretches (3272, 3223 cm^{-1}) and IHB N−H stretch (3107 cm^{-1}) for **G3**. To explain the apparent discrepancies between observed frequencies and calculated IHB N−H stretch and 1°H$_2$O-bonded N−H stretch frequencies, we considered the effects of zero-point vibrations on the position of IHB proton along the shallow intramolecular proton-transfer coordinate as in our previous work.[22] In this method, we performed relaxed potential energy surface scans as a function of the position of IHB proton along the proton transfer coordinate for the remaining degrees of freedom. Harmonic vibrational frequencies were calculated for such optimized geometries without freezing any coordinates to determine the ZPVE-corrected minimum energy geometries and their vibrational frequencies. We believed that the vibrational frequencies of the ZPVE-corrected minimum energy geometries describe better the strongly coupled vibrational modes to the IHB proton-transfer coordinate.

The ZPVE-corrected vibrational spectra for three lowest energy isomers **G1**, **G3**, **G5** at MP2(full)/6-311++G(d,p) are depicted as shaded sticks in Figure 4A, and for comparison the ZPVE-corrected spectra for **G1**, **G2** at B3LYP/6-31+G(d) are also shown in Figure 4B. One thing to notice was that the isomer **G2** converged to the isomer **G5** during the relaxed optimization at MP2(full)/6-311++G(d,p) level, suggesting that almost free rearrangement between two isomers may occur at the zero-point vibrational level, consistent with the similar electronic energies predicted for **G2** and **G5** (Table 1). As shown in Figure 4A, the ZPVE-corrected frequencies for IHB N−H stretch of **G1** and the 1°H$_2$O-bonded N−H stretches of **G3** are much red-shifted from those without ZPVE corrections (3290 → 3244 cm^{-1}; 3272, 3223 → 3250, 3194 cm^{-1}, respectively), reducing the discrepancies between the observed and calculated frequencies. The similar trend for the IHB N−H stretch frequency of **G1** at B3LYP level is shown in Figure 4B.

Conversely, the 3292 cm^{-1} peak of **G5** (Figure 4A) and the

TABLE 4: Many-Body Interaction Analysis of *g*-, *t*-enH$^+$(H$_2$O)$_3$ at MP2(full)/6-311++G(*d,p*)[a]

	G1	G2	G3	G4	G5	T1	T2	T3	T4	T5
					Two-Body					
enH$^+$W$_1$	−15.20	−16.32	−15.81	−12.12	−13.57	−16.41	−17.01	−17.36	−12.33	−15.99
enH$^+$W$_2$	−15.23	−16.72	−16.00	−11.50	−16.81	−16.54	−17.11	−17.08	−12.39	−17.17
enH$^+$W$_3$	−6.63	−17.99	−6.29	−8.85	−16.19	−7.05	−16.83	−6.25	−12.05	−8.70
W$_1$W$_2$	1.75	0.73	0.75	−2.78	0.55	1.79	0.75	0.76	−2.73	0.80
W$_1$W$_3$	−3.60	0.23	−3.60	−2.84	−3.01	−3.58	0.72	−3.56	−2.72	−3.50
W$_2$W$_3$	−3.56	0.61	0.33	−2.69	0.53	−3.54	0.71	0.27	−2.66	0.33
Σ enH$^+$W$_i$	−37.06	−51.03	−38.09	−32.47	−46.56	−40.00	−50.96	−40.69	−36.77	−41.87
Σ W$_i$W$_j$	−5.41	1.57	−2.52	−8.32	−1.93	−5.33	2.18	−2.53	−8.10	−2.37
sum	−42.47	−49.46	−40.61	−40.78	−48.49	−45.33	−48.77	−43.22	−44.88	−44.23
					Three-Body					
enH$^+$W$_1$W$_2$	1.76	1.37	1.48	1.11	1.27	1.95	1.34	1.61	1.05	1.45
enH$^+$W$_1$W$_3$	−1.59	0.96	−2.50	0.26	−0.31	−1.70	1.32	−2.88	1.06	−1.66
enH$^+$W$_2$W$_3$	−1.52	1.14	0.28	1.04	0.87	−1.63	1.31	0.31	1.03	0.39
W$_1$W$_2$W$_3$	0.74	−0.04	0.11	−1.30	−0.05	0.75	−0.04	0.12	−1.16	0.06
Σ enH$^+$W$_i$W$_j$	−1.36	3.47	−0.74	2.42	1.82	−1.38	3.97	−0.97	3.14	0.19
Σ W$_i$W$_j$W$_k$	−0.74	−0.04	0.11	−1.30	−0.05	0.75	−0.04	0.12	−1.16	0.06
sum	−0.62	3.43	−0.63	1.12	1.78	−0.63	3.93	−0.85	1.98	0.25
					Four-Body					
enH$^+$W$_1$W$_2$W$_3$	0.42	−0.07	0.09	−0.05	−0.09	0.46	−0.07	0.06	−0.07	0.03
$E_{\text{Relaxation}}$	1.80	7.26	1.47	2.14	7.65	1.58	0.75	1.31	1.85	1.57
BE$_4$	−40.87	−38.84	−39.69	−37.57	−39.15	−43.92	−44.17	−42.69	−41.11	−42.38
additive	−42.47	−49.46	−40.61	−40.78	−48.49	−45.33	−48.77	−43.22	−44.88	−44.27
nonadditive	−0.20	3.36	−0.54	1.07	1.69	−0.17	3.85	−0.78	1.91	0.28

[a] All values are BSSE-corrected, and units are in kcal/mol. W_i denote numbers of H$_2$O molecules *i* in the clusters according to Figure 1.

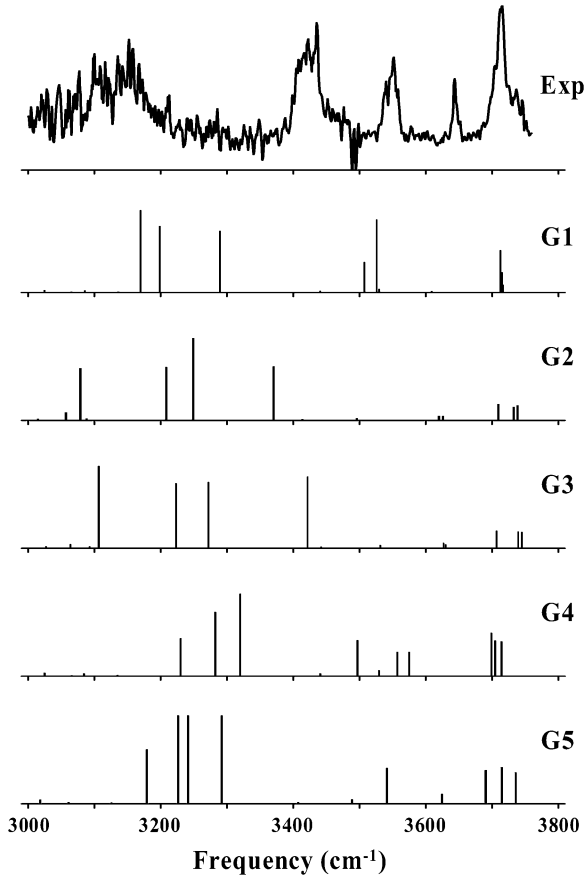

Figure 3. Vibrational predissociation spectrum of *g*-enH$^+$(H$_2$O)$_3$ and ab initio predicted stick spectra for isomers **G1**−**G5** at MP2(full)/6-311++G(d,p).

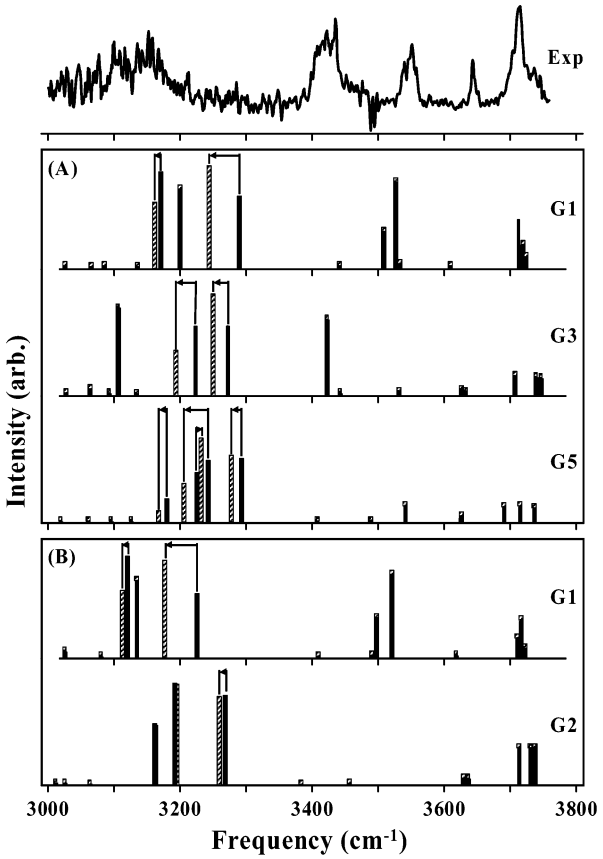

Figure 4. Vibrational predissociation spectrum of *g*-enH$^+$(H$_2$O)$_3$ and ZPVE-corrected vibrational spectra for lowest energy isomers calculated at (A) MP2(full)/6-311++G(d,p); and (B) B3LYP/6-31+G(d). Note that the ZPVE-corrected peaks are denoted as shaded bars.

3268 cm^{-1} peak of **G2** (Figure 4B) assigned to the bonded O−H stretch of H$_2$O(3) molecule participating in the hydrogen bond cage and seven-membered hydrogen bond ring, respectively, were less red-shifted (3277, 3261 cm^{-1}). The remaining discrepancy between the observed and calculated frequencies for **G2**, **G5** may suggest no or lower population of monocyclic tripod isomers (**G2**) and bicyclic tripod isomers (**G5**) in our ion beam, consistent with the results of relative Gibbs free energies at 150 K (Table 2).

D. Many-Body (MB) Interaction Analysis. The origin for the strong IHB-hydration interference in *g*-enH$^+$(H$_2$O)$_3$ was

further investigated by carrying out MB analyses of total hydration energies for *g*-enH$^+$(H$_2$O)$_3$ and *t*-enH$^+$(H$_2$O)$_3$. In the calculation, the total hydration energies were divided into six 2-body (2B), four 3-body (3B), one 4-body (4B) interaction terms, and the relaxation energies for *g*, *t*-enH$^+$ cores and three H$_2$O molecules in the complexes. As shown in Table 4, the trends of the 2B interactions composed of ion−water and water−water interactions between *g*-enH$^+$(H$_2$O)$_3$ and *t*-enH$^+$-(H$_2$O)$_3$ are similar. The tripod isomers (**G2**, **T2**) have the most attractive ion−water 2B interactions (denoted as ΣenH$^+$W$_i$), while the caged isomers (**G4**, **T4**) have the least attractive ion−water 2B interactions due to the geometric constraints. Conversely, the water−water 2B interactions are most attractive for the caged isomers, and slightly repulsive for the tripod isomers. Overall, the contributions of the 2B interactions are greatest for the monocyclic tripod isomer **G2**.

The trends of 3B interactions for *g*-enH$^+$(H$_2$O)$_3$ and *t*-enH$^+$-(H$_2$O)$_3$ are also similar. The cyclic isomers (**G1**, **T1**) and open isomers (**G3**, **T3**) have attractive 3B interactions, while the others have repulsive 3B interactions. Note that the 3B interactions of tripod isomers (**G2**, **T2**) are highly repulsive due to the heterodromic (or bidirectional) hydrogen bond networks.[12] The 4B interaction energies for both complexes are almost negligible except for being slightly repulsive for the cyclic isomers. The overall nonadditive (3B + 4B) interactions for both complexes are slightly attractive for cyclic and open isomers (**G1**, **G3**; **T1**, **T3**), but somewhat repulsive for tripod isomers (**G2**, **T2**). These results, much different from the cases of neutral water clusters (H$_2$O)$_n$ (n = 3−6),[18] suggest that the hydrogen bond cooperativity crucial for forming cyclic-(H$_2$O)$_n$ structures play no role in stabilizing these complexes.

One noticeable difference between *g*-enH$^+$(H$_2$O)$_3$ and *t*-enH$^+$-(H$_2$O)$_3$ was found in their (repulsive) relaxation energies (which measure degree of strains that drive the structural distortion of individual molecules in the complex). The total relaxation energies ($E_{\text{Relaxation}}$) for **G2** and **G5** (~7.5 kcal/mol) are much greater than the other isomers (1−2 kcal/mol) (Table 4) due the large structural distortions resulting from strong IHB−H$_2$O interactions (e.g., $\angle$N$^+$CCN = 71.4°, 67.0°, respectively).[19] Therefore, it is concluded that the greater stability of bicyclic isomer (**G1**) vs monocyclic and bicyclic tripod isomers (**G2**, **G5**) is the consequence of destabilization of the latters by the large relaxation energies and repulsive nonadditive interactions, not the consequence of stabilization of the former by hydrogen bond cooperativity.

IV. Conclusions

This work addresses both vibrational predissociation spectroscopic and ab initio theoretical studies on the structures, interactions, and vibrations of protonated ethylenediamine−(water)$_3$ complexes. The combined results on the interactions between intramolecular hydrogen bonding in ion core and surrounding water molecules suggested the preferential formation of an IHB-assisted bicyclic structure for *g*-enH$^+$(H$_2$O)$_3$. Many-body analyses revealed that the greater stability of the bicyclic isomer (**G1**) vs monocyclic and bicyclic tripod isomers (**G2**, **G5**) for *g*-enH$^+$(H$_2$O)$_3$ was due to the destabilization of the latter by combined large structural distortions arising from strong IHB−1°H$_2$O interactions and repulsive nonadditive interactions. The close correlation between the observed and calculated spectra suggested the coexistence of the bicyclic isomer (**G1**) the and monocyclic open isomer (**G3**) in our beam, consistent with the trend of the calculated Gibbs free energies at 150 K.

Acknowledgment. This work was supported by Korea Research Foundation Grant (KRF-2000-042-D00036), Korea. We also acknowledge the computing time allocations for the SGI Origin-2000 workstation by Department of Mathematics, Yonsei University, Korea.

Supporting Information Available: Geometrical paramters and relative Gibbs free energies for 10 isomers of *g*- and *t*-enH$^+$-(H$_2$O)$_3$. This material is available free of charge via the Internet at http://pubs.acs.org.

References and Notes

(1) Mao, Y.; Ratner, M. A.; Jarrold, M. F. *J. Am. Chem. Soc.* **2000**, *122*, 2950; Woenckhaus, J.; Hudgins, R. R.; Jarrold, M. F. *J. Am. Chem. Soc*. **1997**, *119*, 9586; Frey, P. A.; Whitt, S. A.; Tobin, J. B. *Science* **1994**, *264*, 1927; Cleland, W. W.; Kreevoy, M. M. *Science* **1994**, *264*, 1887.

(2) Cheng, H. P. *J. Phys. Chem*. **1998**, *102*, 6201; Deakyne, C. A. in *Molecular Structure and Energetics*; Liebman, J. F.; Greenberg, A., Eds.; VCH: Berlin, 1987; Vol. 4.

(3) Meot-Ner, M.; Sieck, L. W.; Schneider, S.; Duan, X. *J. Am. Chem. Soc*. **1994**, *116*, 7848; Meot-Ner, M.; Schneider, S.; Yu, W. O. *J. Am. Chem. Soc*. **1998**, *120*, 6980; Meot-Ner, M. in *Molecular Structure and Energetics*; Liebman, J. F.; Greenberg, A., Eds.; VCH: Berlin, 1987; Vol. 4.

(4) Nguyen, V. Q.; Chen, X. G.; Yergey, A. L. *J. Am. Soc. Mass Spectrom*. **1997**, *8*, 1175; Klassen, J. S.; Blades, A. T.; Kebarle, P. *J. Phys. Chem*. **1995**, *99*, 15509.

(5) Jiang, J. C.; Chang, J. C.; Wang, B. C.; Lin, S. H.; Lee, Y. T.; Chang, H. C. *Chem. Phys. Lett.* **1998**, *289*, 373; Jiang, J. C.; Wang, Y. S.; Chang, H. C.; Lin, S. H.; Lee, Y. T.; Niedner-Schatteburg, G.; Chang, H. C. *J. Am. Chem. Soc*. **2000**, *122*, 1398; Yeh, L. I.; Okumura, M.; Myers, J. D.; Price, J. M.; Lee, Y. T. *J. Chem. Phys*. **1989**, *91*, 7319.

(6) Cruzan, J. D.; Braly, L. B.; Liu, K.; Brown, M. G.; Loeser, J. G.; Saykally, R. *Science* **1996**, *271*, 59; Liu, K.; Brown, M. G.; Carter, C.; Saykally, R. J.; Gregory, J. K.; Clary, D. C. *Nature* **1996**, *381*, 501; Estrin, D. A.; Paglieri, L.; Corongiu, G.; Clementi, E. *J. Phys. Chem*. **1996**, *100*, 8701; Liu, K.; Cruzan, J. D.; Saykally, R. J. *Science* **1996**, *271*, 929.

(7) Chaban, G. M.; Jung, J. O.; Gerber, R. B. *J. Phys. Chem. A* **2000**, *104*, 2772; Weber, J. M.; Kelley, J. A.; Nielsen, S. B.; Ayotte, P.; Johnson, M. A. *Science* **2000**, *287*, 2461; Ayotte, P.; Weddle, G. H.; Kim, J.; Johnson, M. A. *Chem. Phys*. **1998**, *239*, 485; Ayotte, P.; Nielsen, S. B.; Weddle, G. H.; Johnson, M. A. *J. Phys. Chem. A* **1999**, *103*, 10665.

(8) Wang, Y. S.; Jiang, J. C.; Cheng, C. L.; Lin, S. H.; Lee, Y. T.; Chang, H. C. *J. Chem. Phys.* **1997**, *107*, 9695; Wang, Y. S.; Chang, H. C.; Jiang, J. C.; Lin, S. H.; Lee, Y. T.; Chang, H. C. *J. Am. Chem. Soc*. **1998**, *120*, 8777.

(9) Boo, D. W.; Chang, H. C.; Lee, Y. T., unpublished results.

(10) Mitsuzuka, A.; Fujii, A.; Ebata, T.; Mikami, N. *J. Chem. Phys*. **1996**, *105*, 2618; Mitsuzuka, A.; Fujii, A.; Ebata, T.; Mikami, N. *J. Phys. Chem. A* **1998**, *102*, 9779; Frost, R. K.; Hagemeister, F. C.; Arrington, C. A.; Schleppenbach, D.; Zwier, T. S. *J. Chem. Phys*. **1996**, *105*, 2605; Bach, A.; Coussan, S.; Muller, A. *J. Chem. Phys*. **2000**, *112*, 1192.

(11) Ikuta, S.; Nomura, O. *J. Mol. Struct.* (*Theochem*) **1987**, *152*, 315; Ikuta, S.; Nomura, O. *Chem. Phys. Lett*. **1989**, *154*, 71; Yamabe, S.; Hirao, K.; Wasada, H. *J. Phys. Chem.* **1992**, *96*, 10261.

(12) Boo, D. W. *Bull. Kor. Chem. Soc*. **2001**, *22*, 693.

(13) Boo, D. W. Ph.D. Thesis, University of California, Berkeley, 1995; Boo, D. W.; Lee, Y. T. *J. Chem. Phys*. **1995**, *103*, 520.

(14) Price, J. M.; Crofton, M. W.; Lee, Y. T. *J. Chem. Phys*. **1989**, *91*, 2749; *J. Phys. Chem*. **1991**, *95*, 2182.

(15) Meot-Ner, M.; Hamlet, P.; Hunter, E. P.; Field, F. H. *J. Am. Chem. Soc*. **1980**, *102*, 6393; Meot-Ner, M. *J. Am. Chem. Soc*. **1984**, *106*, 1265; Yamdagni, R.; Kebarle, P. *J. Am. Chem. Soc*. **1973**, *95*, 3504; Klassen, J. S.; Blades, A. T.; Kebarle, P. *J. Phys. Chem.* **1995**, *99*, 15509.

(16) Frisch, M. J.; et al. GAUSSIAN 98, Gaussian, Inc.: Pittsburgh, Pennsylvania, 1998.

(17) Boys, S. F.; Bernardi, F. *Mol. Phys*. **1970**, *19*, 553.

(18) Hankins, D.; Moskowitz, J. W.; Stillinger, F. H. *J. Chem. Phys*. **1970**, *53*, 4544; Kim, K. S. et al. *Chem. Phys. Lett*. **1986**, *131*, 451; Xantheas, S. S. *J. Chem. Phys*. **1994**, *100*, 7523.

(19) See Supporting Information for geometrical parameters and relative Gibbs free energies.

(20) Jiang, J. C.; Chang, H. C.; Lee, Y. T.; Lin, S. H. *J. Phys. Chem*. **1999**, *103*, 3123.

(21) Kim, K. Y.; Cho, U. I.; Boo, D. W. *Bull. Kor. Chem. Soc*. **2001**, *22*, 597.

(22) Wu, C. C.; Jiang, J. C.; Boo, D. W.; Lin, S. H.; Lee, Y. T.; Chang, H. C. *J. Chem. Phys.* **2000**, *112*, 176.